Submitted to ADVANCED MATERIALS

DOI: 10.1002/adma.201002265

Decoupling local disorder and optical effects in infrared spectra: differentiating between calcites with different origins

By *Kristin M. Poduska*, Lior Regev, Elisabetta Boaretto, Lia Addadi, Steve Weiner, Leeor Kronik,* and *Stefano Curtarolo**

[*] Prof. K. M. Poduska
Memorial University
St. John's, NL A1B 3X7 (Canada)
E-mail: kris@mun.ca
Prof. K. M. Poduska, L. Regev, Dr. E. Boaretto, Prof. L. Addadi, Prof. S. Weiner, Prof. L. Kronik, Prof. S. Curtarolo
Weizmann Institute of Science
76100 Rehovot (Israel)
Dr. E. Boaretto
Bar Ilan University
52900 Ramat Gan (Israel)
Prof. S. Curtarolo
Duke University
Durham, NC 27708 (U.S.A.)
E-mail: stefano@duke.edu

Keywords: Structure-property relations, Infrared spectroscopy, Archaeological science, Biomineralization, Calcium carbonate

Perfect crystallinity is defined as three-dimensional, atomic-level periodic order in a material.[1] The degree of crystallinity can be strongly affected by the specimen's formation process and often plays an important role in its resulting chemical and mechanical properties. Calcium carbonate ($CaCO_3$), for example, exhibits a wide range of gradually changing crystallinity. The two extremes of this range are single-crystalline calcite, which exhibits a single periodic order across macroscopic distances, and amorphous calcium carbonate (ACC),[2] which exhibits a degree of short-range order but a lack of registry between adjacent local units that destroys all long-range periodic order.

In biogenic, geogenic, and anthropogenic materials, variations in crystallinity and local atomic order have each provided valuable insights into material formation pathways.[3] Extracting useful and reliable material structure information, however, usually requires careful and time intensive sample preparation and often highly specialized equipment. Here,

we show that routine IR spectroscopy can reveal subtle differences in the degree of local disorder among different sources of crystalline calcite quickly and easily by decoupling two competing contributions to spectral peaks: particle-size-dependent optical absorption and local atomic order. Our method is particularly powerful because no direct measurement of particle size is required and because the analysis strategy can be readily generalized for use with other IR-active solid materials.

In general, solid materials possess optical phonons that correspond to intra-unit cell vibrational modes. When probed with IR light, they lead to absorption peaks whose frequencies each vary slightly depending on the specimen size, shape, and the polarization of the incident light.[4] Thus, the phonon mode may be manifested as a broad and complex IR absorption peak due to phonon-optical coupling (polariton) contributions from bulk, surface, transverse and longitudinal optical modes. Theoretical studies show that peak shapes become much simpler, supporting only a single optical surface (Frölich) mode, once the size of a specimen's particles are too small to support wave-like (bulk) polariton modes.[5] Nevertheless, prediction of peak shapes and intensities can be complicated by other effects, such as particle aggregation and scattering. The challenge is especially pronounced for polycrystalline materials because it is impractical to assess routinely and quantitatively the particle sizes and their aggregation. Such specimens, typically hand-ground and dispersed in an IR-transparent matrix like KBr, are the norm for assessing polymorph and atomic-level structural information in the context of archaeology, geology, and materials/biomaterials science.[2,6] Mie scattering theory (which assumes small spherical particles that are well separated) and Hapke theory (based on large, irregular particles in close proximity) have each been invoked to account for aggregation and scattering effects, but a comprehensive quantitative model has yet to be introduced.[7] Thus, the question of associating changes in IR peaks with material-related changes in local order – distinct from the influences of scattering and aggregation – persists.

To answer this question, we looked at calcite as an interesting and broadly applicable test case that is of particular relevance to materials science. Qualitative features of transmission IR spectra are the same among geogenic, pyrogenic, and laboratory synthesized calcites in the small particle (Frölich) limit.[8] Calcite has three symmetry-allowed phonon modes in the mid-IR range: 713 cm^{-1} (ν_4, in-plane CO_3 bend), 874 cm^{-1} (ν_2, out-of-plane CO_3 bend), and 1420 cm^{-1} (ν_3, asymmetric CO_3 stretch).[9] As a specimen is subjected to more grinding, IR peaks sharpen to yield both higher intensities and smaller full-width half-maximum (FWHM) values, but the mode frequencies remain constant (**Figure 1a**). A specimen can be reground and re-pressed repeatedly before the FWHM reaches a limiting value. The limiting values, as well as the starting widths, vary among different sources of calcite specimens. Earlier studies showed that peak height ratios facilitate comparison among spectra from different specimens,[8] and that calcite bending modes are particularly sensitive to local coordination environment.[10] Importantly, a comparison of peak width and height ratios of the ν_2 and ν_4 bending modes for all calcites (**Figure 1b**) shows a strong inverse correlation. This allows us to address peak sharpening in terms of relative peak height changes in subsequent comparisons.

It is tempting to think of grinding-induced IR peak sharpening as an indication that the local calcite CO_3 environments are becoming more ordered with correspondingly less dispersion in their characteristic vibrational energies. However, we can rule out the possibility of grinding-induced local ordering by correlating several observations. First, particle-size-related peak sharpening is a general – but often overlooked – phenomenon that has been documented for a wide range of materials.[5,11] Second, we confirmed that these effects occur not only in materials comprised of macroscopic single crystals (such as calcite spar), but also for amorphous materials such as silica glass. This means that mechanical factors, such as heat-induced annealing or strain release during grinding, would be difficult to invoke as consistent explanations for ordering in both highly crystalline and poorly crystalline materials.

Third, explanations related to reorganized surface structures during grinding would be relevant only for surface-to-volume ratios that involve more than ~5% of the material volume; this would require particles << 100 nm, which are exceedingly difficult to achieve with hand-ground specimens. We therefore conclude that the dominant contribution to the peak sharpening displayed in Figure 1 cannot be related to an increase in the local atomic order. Instead, we propose that optical interactions with the sample dominate this effect.

The key to isolating the contribution of optical effects to peak sharpening is in comparing peak intensities within a single IR spectrum. When a calcite-KBr pellet is reground multiple times, each grinding reduces particle sizes and homogenizes the distribution of calcite within the KBr mixture. Intensity plots, normalized to the largest (ν_3) peak for ease of comparison among pellets from different grinding experiment,[8] show monotonically decreasing ν_2/ν_3 and ν_4/ν_3 peak height ratios with each grinding step. (We emphasize that these ratios decrease because the ν_3 peak sharpens faster than both the ν_2 and the ν_4 peaks, as shown in Figure 1a). **Figure 2a** shows that the trend in this "grinding curve" can be quantitatively reproduced with a simple calculation relating particle size to total pellet absorption. One can model an IR specimen as a disc of height *h* that contains monodisperse calcite particles distributed within an IR-transparent matrix[11] (see Supporting Information S1). Single calcite particles with size *d* will transmit a fraction *i(d)* of the IR light incident upon them, while the KBr will transmit all IR. For ease of calculation, we partition the pellet into layers of uniform thickness, *h/d*. The transmittance *t* for a single layer will depend on the calcite fraction *f,* which is assumed to be uniform throughout the pellet and remains constant with grinding. Thus, the transmittance can be described as a sum of the KBr fraction [1-*f*] that transmits 100% of incoming IR light and the calcite fraction *f* that transmits a fraction *i(d)* of the incident light: $t(d) = [[1-f] + f\ i(d)]$. The entire pellet will have transmittance $T = t^{h/d}$. Relating transmittance to absorbance, *A*, we see that $A = \log [1/T] = - [h/d] \log [[1-f] + f\ i(d)]$. Each IR mode will have a different, experimentally determined true absorption coefficient *k*

that, along with the particle shape and size, affects the single particle transmission fraction *i*. For example, approximating the predominantly rhombohedral calcite crystallites as cubes yields $i(d) = \exp[-k\,d]$, where the ν_3 mode has $k = 3.5\ \mu m^{-1}$, ν_2 has $k = 1.0\ \mu m^{-1}$, and ν_4 has $k = 0.3\ \mu m^{-1}$.[11] The end result is somewhat counterintuitive: a smaller particle absorbs less light on its own, but an ensemble of smaller particles leads to greater overall absorption with decreasing particle size, because of a more uniform distribution of material within the matrix. Utilizing peak intensity ratios (Figure 2) eliminates the explicit *h/d* dependence. Furthermore, Figure 2a shows that different assumptions about particle shape do not change the qualitative trend of the simulated grinding curves and do not even show quantitative influence for the smallest and largest values of *d*. Thus, plots of absorbance intensity ratios are a surprisingly robust way to mitigate particle shape effects in IR spectral analyses. Note that the mechanism described here illustrates only *one* means through which grinding curves can come about. There are undoubtedly other factors, notably photon-phonon coupling, that may be needed to understand the phenonmenon more deeply. The salient point here is that the particle-size-dependence of the spectrum can be considered systematically *via* repeated grinding.

Figure 2b shows that different sources of calcite localize to distinct grinding curves, and that each curve is qualitatively consistent with the small-diameter (small ν_4/ν_3) portion of the simulated grinding curve. Earlier studies demonstrated that high percentages of amorphous material cause drastic IR peak widening in biogenic calcium carbonates,[10] but the calcites considered here (with the exception of the poorly crystallized calcite from ACC precursors) do not show evidence of amorphous phases. Here, powder X-ray diffraction (XRD) measurements on uniformly ground and sieved specimens show sharp diffraction peaks that are typically ascribed to well-crystallized materials. However, there are subtle differences in the crystalline order of calcites from different sources (see Supporting Information S2). XRD peak widths, which are sensitive to the size of coherent domains within the crystallites, are noticeably larger for plasters than for geogenic limestone or calcite spar. These broader

plaster XRD peak widths, which indicate decreased long-range order, correlate with the comparatively broader FTIR peak widths, which suggest decreased short-range order. Nevertheless, these relatively small differences in crystallinity appear to underlie the grinding curve shifts shown in Figure 2b.

To confirm that differences in local (dis)order are consistent with the observed offsets to the IR grinding curves, we performed first-principles calculations of calcite phonon frequencies as follows. First, to mimic disorder we induced distortions of the unit cell geometry by changing the rhombohedral angle α while conserving cell volume, with subsequent atomic relaxation. Then, for each value of α we calculated all phonon frequencies. Because the observed IR spectra correspond to localized vibrations that are insensitive to long-range order, it is possible to simulate the experimental IR spectra by averaging over the vibrational spectra obtained from an ensemble of distorted unit cells.[10] Specifically, we simulated disorder by assuming an effective disorder temperature, T_{dis}, and a corresponding canonical probability distribution of the rhombohedral angle, $p(\alpha) \sim \exp(\delta E(\alpha)/kT_{\mathrm{dis}})$. One can artificially increase the degree of disorder by increasing T_{dis}. We used disorder temperatures of 20, 76, and 514 K, which correspond to a standard deviation in α of 1.05, 2.05 and 5.33°, respectively. These local distortions, being random in nature, average out over a great number of unit cells so that they need not result in appreciable macroscopic deformations.

Figure 3a shows that the introduction of disorder (increasing T_{dis}) leads to lower maximum peak intensities and larger FWHM values. More importantly, small to moderate T_{dis} values induce this broadening without any significant shift in the overall peak frequencies, consistent with the experimental observations (Figure 1b). Peak broadening is most pronounced for the ν_3 mode because of the larger magnitude of the convexity of ν_3 *vs.* $\delta\alpha$ curve (**Figure 3b**). More disorder (increasing T_{dis}) also moves the loci of peak height ratios

(ν_4/ν_3 and ν_2/ν_3) further away from the perfect crystalline case in a direction that matches qualitatively the shifts in the experimental grinding curves (**Figure 3c,d**).

By combining the results of the local disorder calculations with the grinding curve analyses, we conclude that two factors affect IR peak intensities in a diametrically opposed, and clearly distinguishable, manner. The characteristic *shape* of a single grinding curve is dominated by relative changes in absorption due to different particle sizes (Figure 2a). The *offset* of a grinding curve, relative to the simulated ideal behavior (Figure 3c,d), provides information about the degree of local crystalline order. Spectra from specimens with the highest degree of long-range order (the geogenic spar and the laboratory-synthesized annealed calcite) are in excellent agreement with simulated intensity ratios at small particle sizes. At the other extreme is poorly crystallized calcite, formed from an amorphous calcium carbonate precursor (ACC), with a grinding curve that is the most displaced. We emphasize that particle size differences can cause much larger changes in peak intensities than do differences in local order; thus, grinding curves are useful for distinguishing between these competing effects.

There are three factors that make the IR peak analysis approach both unique and powerful. First, the peak ratio analysis is quite general and can likely be extended to a broad range of materials beyond the calcite test case described here. Particle-size-related peak sharpening has been documented for a wide range of materials[5,11] and exploiting this phenomenon in simulated grinding curves requires only one kind of material-specific parameter: the true extinction coefficient for each mode of interest. In fact, we observe similar effects in the IR spectra of aragonite (also a calcium carbonate polymorph), silica, and carbonated hydroxyapatite from bones. Second, this analysis method decouples particle size effects from other IR spectral features without any requirements for a direct measurement of particle size. This makes it a viable analysis for routinely acquired IR spectra, including hand-ground samples where particle sizes and distributions are challenging and time-consuming to assess. (We also note that spectra from well-ground samples localize near the end of the

grinding curves where further grindings have relatively little affect on the analyzed peak ratios. Therefore, well-ground samples produce reproducible spectra and can be compared with results of earlier investigations.[2,3]) Third, this analysis offers a way to compare the degree of crystalline order quickly, and with very little sample (~ μg amounts) compared to other standard methods such as powder X-ray diffraction peak widths. Materials science, archaeology and biomineralization are disciplines that can benefit from this technique for using crystallinity as an indicator for different pathways of material formation. For example, this method will complement previous studies that have identified ACC precursors during biomineralization processes[2,3] because it can facilitate comparisons of crystallinity at different stages of the conversion from ACC to calcite.

Experimental and Computational Details

Samples were prepared from hand-ground (agate mortar and pestle, 10 s to 3 min) calcite that was diluted (~1:20 mass ratio) with KBr (Sigma-Aldrich, FTIR grade), then uniaxially pressed (2 tons, sufficient to allow the KBr to flow and recrystallize as an IR transparent matrix [12]) to yield a disk that is suitable for IR measurements in a transmission geometry (Nicolet 380, 4 cm^{-1} resolution). We applied this procedure to geogenic single crystalline calcite (Iceland spar, Ward's), geogenic limestones (Nesher Israel Cement Enterprises Ltd., Tell es-Safi/Gath (Israel), and Yiftahel (Israel)), plasters (laboratory calcined and slaked chalky limestone aged for 2 years [8], and repair plaster to the Holy Sepulcher Church bell tower (Jerusalem, Israel) aged for 7 years), and laboratory synthesized calcite nanoparticles. Nanoparticles were prepared from $CaCl_2$ and Na_2CO_3 (1 M, ice-bath cooled, from Sigma salts) that were mixed to 50 mM. The solution was placed immediately on a membrane filter, washed with absolute ethanol, and dried under a heat lamp. Precipitates were either measured immediately (denoted “from ACC precursor”) or annealed at 400 °C for 2 h prior to measurement. Complete quantification of particle size is non-trivial, but analyses of scanning

electron micrographs (see Supporting Information S3) show that starting particle diameters for the spar change from a median value above 5 μm to near 0.5 μm, depending on grinding (with a non-normal distribution biased towards smaller sizes), while calcite from ACC precursor are substantially smaller (80 ± 30 nm), even when annealed (200 ± 100 nm). Refinements of XRD peak positions (see Supporting Information S2) show that geogenic and pyrogenic samples have lattice constants that compare well with standard values for calcite.

First-principle calculations of calcite phonon frequencies were based on standard methods described elsewhere [10,13]. Density functional calculations were performed with the *ab initio* package VASP within the LDA approximation [14]. Vibrational properties were calculated with the high-throughput framework AFLOW-phonons [15].

Acknowledgements

We thank Eugenia Klein (scanning electron microscopy), Yishai Feldman (XRD), and Assaf Gal (ACC synthesis protocol) for their assistance, and support from the Kimmel Center for Archaeological Science, Weizmann Institute. L.A. is the incumbent of the Dorothy and Patrick Gorman Professorial Chair of Biological Ultrastructure, S.W. is the incumbent of the Dr. Trude Burchardt Professorial Chair of Structural Biology, L. K. acknowledges support by the Lise Meitner Minerva Center for Computational Quantum Chemistry, and S.C. acknowledges the Feinberg Fellowship support at the Weizmann Institute. Supporting Information is available online from Wiley InterScience or from the authors.

Received: ((will be filled in by the editorial staff))
Revised: ((will be filled in by the editorial staff))
Published online: ((will be filled in by the editorial staff))

[1] G. Allegra, P. Corradini, H.-G. Elias, P.H. Geil, H.D. Keith, B. Wunderlich, *Pure Appl. Chem.* **1989**, *61*, 769.
[2] a) D. Gebauer, A. Völkel, H. Cölfen, *Science* **2008**, *322*, 1819; b) D. Wang, A.F. Wallace, J.J. de Yoreo, P.M. Dove, *Proc. Natl. Acad. Sci. USA* **2009**, *106*, 21511; c) L. Addadi, S. Raz, S. Weiner, *Adv. Mater.* **2003**, *15*, 959.
[3] a) B. Pokroy, A. Fitch, E. Zolotoyabko, *Adv. Mater.* **2006**, *18*, 2363; b) Y. Politi, R.A. Metzler, M. Abrecht, B. Gilbert, F.H. Wilt, I. Sagi, L. Addadi, S. Weiner, P.U.P.A. Gilbert, *Proc. Natl. Acad. Sci. USA* **2008**, *105*, 17362.
[4] T.G. Mayerhöfer, *Vib. Spectrosc.* **2004**, *35*, 67.
[5] R. Ruppin, R. Englman, *Rep. Prog. Phys.* **1970.** *33*, 149.
[6] S. Weiner, *Microarchaeology: beyond the visible record*, Cambridge University Press, Cambridge **2010**, Ch. 12.
[7] J.E. Moersch, P.R. Christensen, *J. Geophys. Res.* **1995**, *100*, 7465.
[8] a) V. Chu, L. Regev, S. Weiner, E. Boaretto, *J. Archaeol. Sci.* **2008.** *35*, 905; b) L. Regev, K.M. Poduska, L. Addadi, S. Weiner, E. Boaretto*, J. Archaeol. Sci.* **2010** *37,* 3022.
[9] W.B. White in *Infrared Spectra of Minerals* (ed. V. Farmer), Mineralological Society of Great Britain and Ireland, London **1974**, Ch.12.
[10] R. Gueta, A. Natan, L. Addadi, S. Weiner, K. Refson, L. Kronik, *Angew. Chem. Int. Ed.* **2007**, *46*, 291.
[11] G. Duyckaerts, *Analyst* **1959**, *84*, 210.
[12] A.J. Blanch, J.S. Quinton, C.E. Lenehan, A. Pring, *Anal. Chim. Acta* **2007**, *590*, 145.
[13] L. Valenzano, F.J. Torres, K. Doll, F. Pascale, C.M. Zicovich-Wilson, R. Dovesi, *Z. Phys. Chem.* **2006**, *220*, 893.
[14] G. Kresse, J. Hafner, *Phys. Rev. B* **1993**, *47*, 558.
[15] a) S. Curtarolo, D. Morgan, W. Setyawan, R. Chepulskyy, G. Hart, O. Levy, AFLOW: software for high-throughput calculation of material properties, http://materials.duke.edu/aflow.html, **2010**; b) W. Setyawan, S. Curtarolo, *Comp. Mater. Sci.* **2010.** *49*, 299.

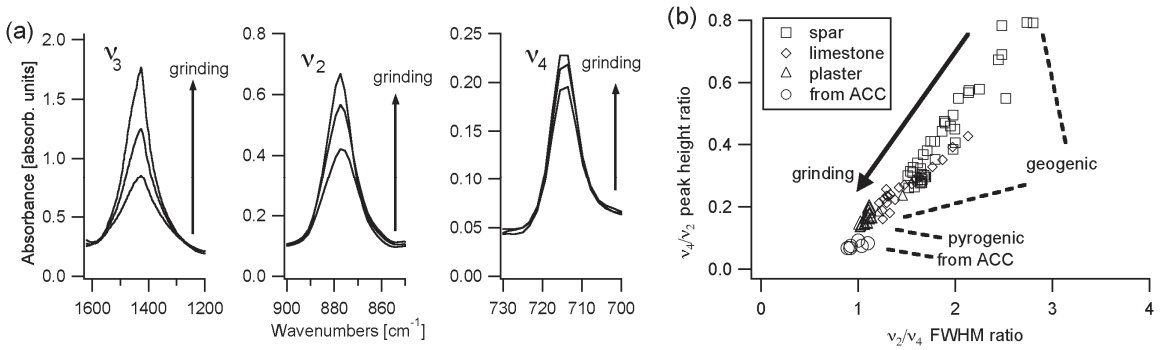

Figure 1. (a) FTIR spectra for geogenic calcite (chalky limestone) illustrate that peak sharpening occurs with grinding, leaving peak positions unchanged. A single specimen was ground and re-pressed; spectra are shown as-collected with no scaling. With grinding, the ν_3 peak sharpens more than ν_2, which sharpens more than ν_4. Peak areas also increase slightly with grinding. (b) Peak intensity ratios (defined as ν_4/ν_2) and FWHM ratios (defined as ν_2/ν_4) follow a linear relation for all calcite specimens; each data point corresponds to a single spectrum. The trend with increased grinding is denoted with an arrow.

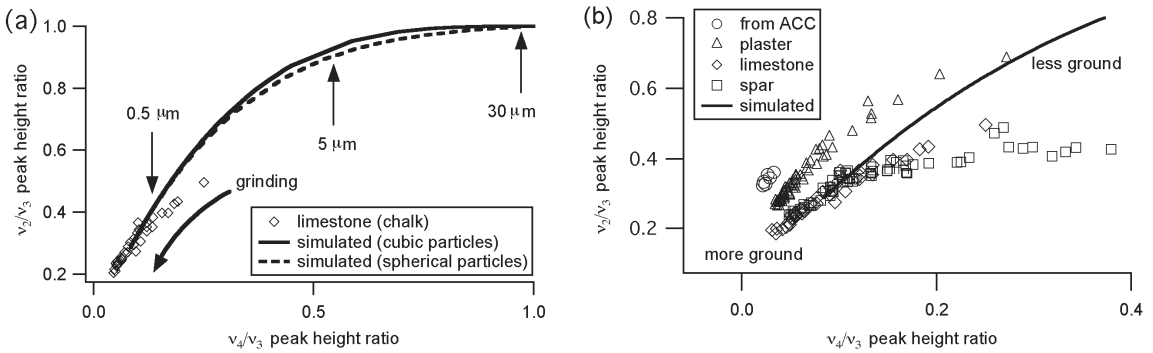

Figure 2. (a) Simulated peak intensity ratios (ν_2/ν_3 *vs.* ν_4/ν_3) based on particle-size-dependent absorption values for calcite (solid and dashed lines) compared with representative "grinding curve" data for chalky limestone (diamonds). Simulations assume a calcite filling fraction f = 0.05, in line with experiments. Selected particle sizes (d = 0.5, 5, and 30 μm) used for the simulations are noted on the plot. Quantitative agreement between simulation and experimental data occurs for smaller particle sizes and well-ground samples. (b) An enlarged view shows that experimental grinding curves are distinct for calcites whose origins are geogenic (spar and limestone), pyrogenic (plaster) or synthetic (from ACC precursors). The data include samples exposed to either multiple grindings or different levels of initial grinding. The simulated grinding curve for cubic particles (solid line) is shown for comparison.

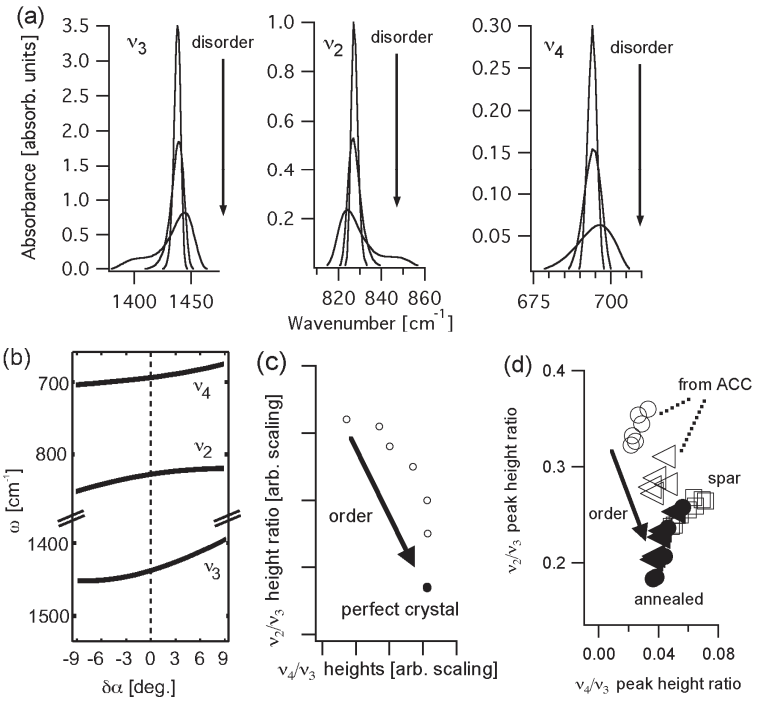

Figure 3. (a) Simulations show that ν_4, ν_2 and ν_3 peaks broaden with increasing disorder (introduced through an effective temperature T_{dis}). This is because phonon frequencies (b) change according to the amount of local distortion induced by small changes in the rhombohedral angle α. (c) Simulated peak height ratios change with disorder in a way that is consistent with (d) the experimental grinding curve shifts. In (c), the ratio for a simulated perfect crystal (no disorder) is indicated by a solid circle, and there is an implicit scaling factor based on the choice of initial peak width for the simulated spectra. The experimental data in (d) show that when poorly crystallized laboratory-synthesized calcite samples (open circles and triangles) are annealed (solid circles and triangles), their grinding curves shift to coincide with that for highly crystalline spar calcite (open squares).

Table of contents entry

Infrared spectral peak *broadening* due to atomic disorder and *narrowing* due to particle-size-related optical absorption effects can be decoupled experimentally and theoretically. Applied to different sources of polycrystalline calcite, the method provides a powerful diagnostic tool for archaeology, geology, and materials/biomaterials science.

Keyword: Structure-property relations

Kristin M. Poduska*, Lior Regev, Elisabetta Boaretto, Lia Addadi, Steve Weiner, Leeor Kronik and Stefano Curtarolo*

Decoupling local disorder and optical effects in infrared spectra: differentiating between calcites with different origins

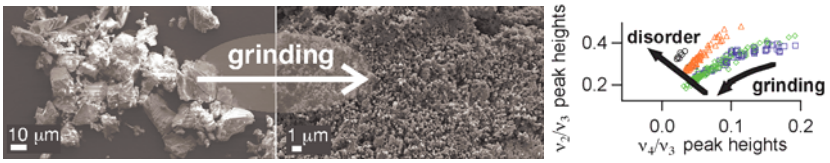

Submitted to ADVANCED MATERIALS

Supporting Information

Decoupling local disorder and optical effects in infrared spectra: differentiating between calcites with different origins

By *Kristin M. Poduska*, Lior Regev, Elisabetta Boaretto, Lia Addadi, Steve Weiner, Leeor Kronik* and *Stefano Curtarolo**

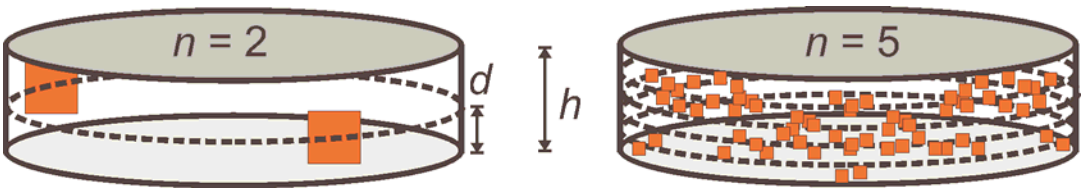

Figure S1. Schematic diagrams of monodisperse calcite particles (red squares) within an IR-transparent cylindrical KBr pellet. The pellet can be modeled as a stack of thin cylindrical layers (denoted by dotted lines) whose thicknesses are defined by the particle diameter d. Thus, the pellet has a thickness $h = n\,d$. Grinding does not change pellet volume or calcite filling fraction f. However, grinding does produce smaller particles. Pellet absorption A scales as $A = -(h/d) \log[(1-f) + f\,i]$, where i is the transmission through a single particle. Thus, pellet absorption is a particle-size-dependent quantity.

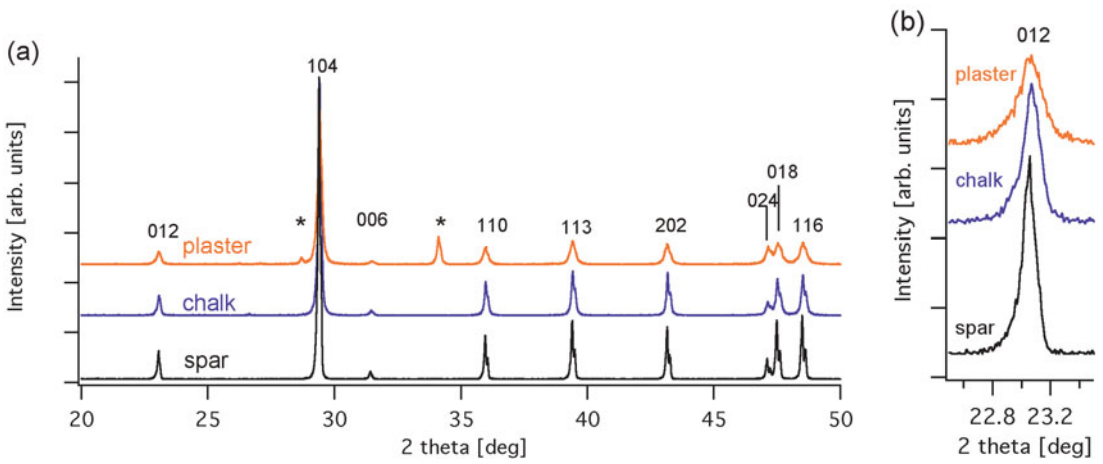

Figure S2. (a) Comparison of indexed powder X-ray diffraction patterns for calcites from different sources. All samples show sharp diffraction peaks, but (b) shows that the plaster calcite peaks are perceptibly broader than those for spar or chalk. Lattice constant refinements show good agreement with values expected for calcite: JCPDS standard 05-0586 (a = 4.990 Å, c = 17.062 Å), spar calcite (a = 4.991(4) Å, c = 17.067(5) Å, chalk (a =4.994(5) Å, c = 17.05(1) Å), and plaster (a = 4.988(6) Å, c = 17.06(1) Å). The plaster slaking process produces $Ca(OH)_2$; some of this phase remains in the plaster, and is denoted with asterisks (*).

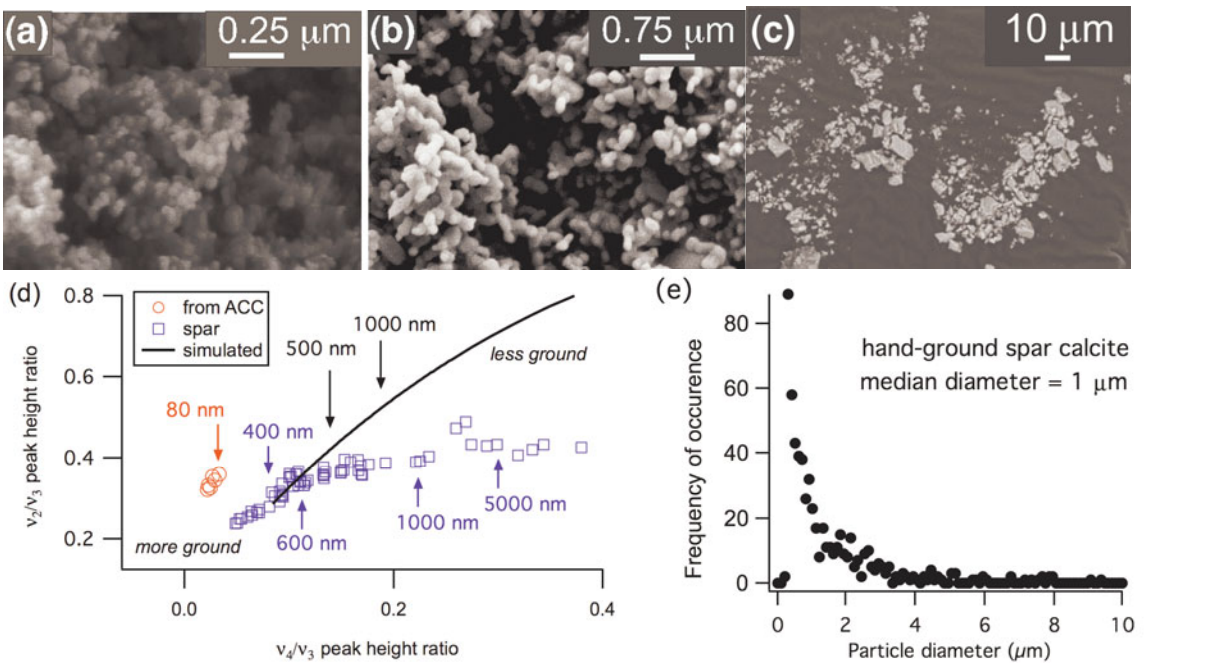

Figure S3. Representative scanning electron micrographs showing examples of the range of starting particle sizes for nanoparticle calcite from an ACC precursor (a) as-prepared (80 ± 30 nm) and (b) after annealing for 2 hours at 400°C (200 ± 100 nm). Hand-ground calcite spar is shown in (c) and displays larger particles sizes along with a much larger dispersion in sizes. Plot (d) provides comparisons of median starting particle sizes for as-prepared calcite (red circles, corresponding to (a)), different grindings of the calcite spar (blue squares, corresponding to (d)) with the simulated grinding curve (solid black line). Complete quantification of particle sizes and their distribution is non-trivial because the grinding process yields a non-normal distribution of particle sizes as shown in (e) (based on image (c)).